Probing intrinsic transport properties of single metal nanowires: Direct-write contact formation using a focused ion beam

G. De Marzi, D. Iacopino, A. J. Quinn, and G. Redmond

Citation: Journal of Applied Physics **96**, 3458 (2004); doi: 10.1063/1.1779972
View online: http://dx.doi.org/10.1063/1.1779972
View Table of Contents: http://aip.scitation.org/toc/jap/96/6
Published by the American Institute of Physics

Probing intrinsic transport properties of single metal nanowires: Direct-write contact formation using a focused ion beam

G. De Marzi, D. Iacopino, A. J. Quinn, and G. Redmond[a)]
Nanotechnology Group, NMRC, Lee Maltings, Prospect Row, Cork, Ireland

(Received 12 March 2004; accepted 14 June 2004)

The transport characteristics of 70-nm-diameter platinum nanowires (NWs), fabricated using a pore-templated electrodeposition process and individually contacted using a focused ion beam (FIB) method, are reported. This approach yields nanowire devices with low contact resistances ($\sim$400 Ω) and linear current–voltage characteristics for current densities up to 65 kA/cm^2. The intrinsic nanowire resistivity (33 ± 5 $\mu\Omega$ cm) indicates significant contributions from surface- and grain-boundary scattering mechanisms. Fits to the temperature dependence of the intrinsic NW resistance confirm that grain-boundary scattering dominates surface scattering (by more than a factor of 2) at all temperatures. Our results demonstrate that FIB presents a rapid and flexible method for the formation of low-resistance ohmic contacts to individual metal nanowires, allowing intrinsic nanowire transport properties to be probed. © *2004 American Institute of Physics*. [DOI: 10.1063/1.1779972]

I. INTRODUCTION

Metallic nanowires (NWs) have been proposed as being potentially important in the development of nanoelectronic devices based on bottom-up fabrication.[1,2] In this regard, it is important to establish a method for rapid, flexible contacting and characterization of nanowire-based electronic devices. Electrical contacts are generally overlaid onto individual nanowires using optical- or electron-beam lithography-based methods.[3,4] Focused ion beam (FIB) methods have been used recently to make contacts to multiwalled carbon nanotubes and semimetallic Bi NWs with some success.[5,6] In this paper, we report a general method for rapid fabrication of low-resistance electrical contacts to metallic NWs, in which a FIB system is employed for a direct write of electrical contacts to nanowires assembled onto larger micron-scale electrodes. Using this approach, the charge-transport properties of single 70-nm-diameter platinum nanowires (Pt NWs) are probed in depth using variable-temperature electrical characterization.

II. NANOWIRE FABRICATION

Platinum nanowires are fabricated in commercial polycarbonate matrices (Poretics, Osmonics Inc., 50 nm nominal pore diameter) by the method of pore-templated electrodeposition.[7] A gold layer is sputtered onto one side of the membrane and serves as the working electrode in a standard three-electrode electrochemical cell. The NW electrodeposition is carried out at −0.3 V relative to a standard calomel reference electrode, with a Pt rod serving as the counterelectrode. The employed electrolyte consists of 2% H_2PtCl_6 in de-ionized water ($>$18 MΩ). After pore filling by electroplating, the template is removed from the electrochemical cell and dissolved in dichloromethane. The freed NWs are then cleaned using an ultrasonic bath and further purified by centrifugation. Scanning electron microscopy (SEM) images of the Pt NWs confirm that the NWs are cylindrical in shape, with a diameter of 70 ± 5 nm and with lengths up to 5 μm. Figure 1(a) shows a high-resolution SEM (HRSEM) image of a 70-nm-diameter polycrystalline

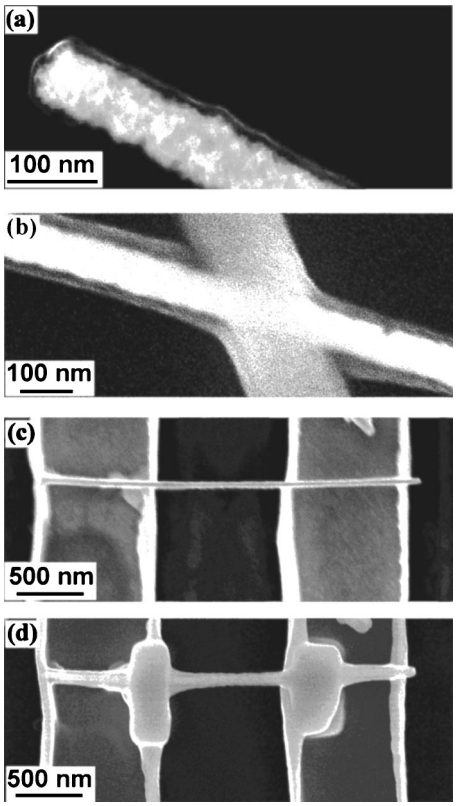

FIG. 1. (a) High-resolution SEM image showing a NW with polycarbonate membrane coating; (b) after FIB deposition of interconnects, the membrane is partially degraded, but the NW is not damaged; (c) SEM image of a Pt NW deposited onto Au electrical contacts; (d) the NW is then contacted by direct write of platinum metal junction contacts using a focused ion beam. The apparent wire width broadening is due to melting of the residual polycarbonate membrane, which surrounds the NW.

[a)]Electronic mail: gredmond@nmrc.ie

Pt NW. A thin-film layer surrounds the NW. We believe this comprises residual polycarbonate material from the porous membrane template.[8] Repeated HRSEM imaging or FIB deposition of metal junction contacts onto the NW results in partial degradation of this membrane material [Fig. 1(b)].

Parallel planar Ti/Au microelectrodes are fabricated on Si/SiO_2 chip substrates (n-Si wafers with 500 nm thermal SiO_2) using UV lithography, metal evaporation, and liftoff, with interelectrode gaps ranging from 1 to 5 μm. The thickness of the deposited gold in these contacts is 20 nm (plus 5 nm Ti adhesion layer) with a measured sheet resistance of 33 Ω/sq, so that the resistance of the microelectrode tracks (R_{track}) was estimated to be about 130 Ω.

III. ROOM-TEMPERATURE ELECTRICAL CHARACTERIZATION

A. Experimental setup

Room-temperature transport measurements are performed on NWs drop-deposited onto parallel microelectrodes in a two-point geometry by sweeping the bias voltage applied to the NW (−1.5–1.5 mV) and recording the current with picoampere resolution. Variable-temperature measurements (4–300 K) are performed using a He-bath cryostat on NW-bearing chips wire bonded to leadless chip carriers.

B. Direct-write contacts: FIB

Initial electrical characterization of single Pt NWs drop-deposited on the microelectrodes [Fig. 1(c)] yields room-temperature resistance values in excess of 1 GΩ for biases of 1 mV, attributed to the insulating residual polycarbonate layer surrounding the NWs [Fig. 1(a)]. To form lower-resistance contacts between the NWs and the electrodes, a FIB system (FEI Vectra 200DE, 30 keV Ga ions, and 10 nm nominal spot diameter) is therefore employed for imaging, local polycarbonate layer removal, and direct write of the electrical junction contacts between the NWs and the microelectrodes [Fig. 1(d)]. It is important to minimize exposure of the NWs and the microelectrodes to the highly energetic Ga ion beam because the beam can damage the surface and increase the measured resistivity of the junction contact.[9] However, at least one FIB image is necessary for alignment purposes. All junction contacts are fabricated under the same experimental conditions (10 pA beam current, 30 kV acceleration voltage). In the inset of Fig. 2, the room-temperature current–voltage (I–V) characteristic of a single 70-nm-diameter, 2.8-μm-long Pt NW contacted by FIB is reported. The trace is ohmic for current densities up to 65 kA/cm^2 (a value higher than that recently measured for 60-nm-diameter Cu NWs, $\approx$7 kA/cm^2).[4]

C. Evaluation of the intrinsic nanowire resistivity and the contact resistance

In order to evaluate the intrinsic NW resistivity, ρ_{NW}, a series of single NW devices was fabricated. For each device, the mean room-temperature resistance, R_{meas}, was calculated by averaging the inverse slopes of several measured I–V curves, and the effective NW length, L (distance between the FIB contacts), was measured by SEM. The intrinsic nanowire resistivity, ρ_{NW}, can be extracted from a linear fit of R_{meas} vs L, i.e., $R_{meas}=R_{cont}+\rho_{NW}L/A$, where R_{cont} is the contact resistance, and A is the NW cross-sectional area. The slope of the fit (solid line in Fig. 2) yields $\rho_{NW}=33\pm5$ $\mu\Omega$ cm. A relative resistivity ratio is defined as $\rho_{rel}=\rho_{NW}/\rho_{Bulk}$ ($\rho_{Bulk}=10.7$ $\mu\Omega$ cm for Pt), yielding $\rho_{rel}^{Pt}=3$, consistent with the literature reports for 60-nm-diameter Cu and 70-nm-diameter Au NWs ($\rho_{rel}^{Cu}=10$ and $\rho_{rel}^{Au}=2$, respectively).[3,4] This enhanced ratio value can be attributed to both the surface- and the grain-boundary scattering mechanisms operating within the Pt NWs. This suggestion will be discussed in more detail later. From the fit intercept value, a (constant) contact resistance $R_{cont}=R_{FIB}+R_{track}=405\pm35$ Ω may be estimated. Taking $R_{track}=130$ Ω, the room-temperature resistance of the FIB junction contacts (R_{FIB}) is estimated to be 275 Ω. The linearity of the I–V curves, as well as the relatively low value of the contact resistance, demonstrates the efficiency of FIB as a contacting method.

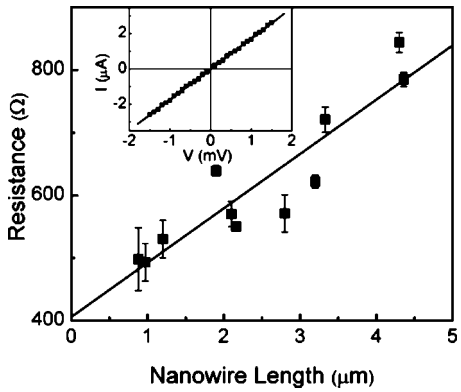

FIG. 2. Mean room-temperature resistance vs NW length for the FIB contacted 70-nm-diameter Pt NWs. The intrinsic NW resistivity is $\rho_{NW}=33\pm5$ $\mu\Omega$ cm, extracted from the slope of the linear fit (solid line). The contact resistance is $R_{cont}=405\pm35$ Ω (intercept value). Inset: room-temperature I–V characteristic of a 70-nm-diameter, 2.8-μm-long FIB-contacted Pt NW. The linear fit demonstrates ohmic behavior for current densities up to 65 kA/cm^2.

IV. VARIABLE-TEMPERATURE ELECTRICAL CHARACTERIZATION

A. The FIB contact contribution to the measured resistance

Variable-temperature electrical characterization was undertaken to gain insight into the possible contributions of the different scattering mechanisms within the NWs. For this purpose, the FIB junction contact resistivity was evaluated because a contribution from the disordered Pt metal compound deposited by the FIB system is expected.[10] To this end, a series of FIB-written individual test wires of different lengths ($L=2.0$–6.5 μm) and cross sections ($A=0.02$–0.32 μm^2) were first written between parallel Au microelectrodes [see the inset in Fig. 3(b) for a typical example]. The measured resistance values are plotted in Fig. 3(a) as a function of L/A whereas in the inset of Fig. 3(a), the room-temperature (I–V) characteristic of a 0.06 μm^2 cross-sectional area, 2-μm-long FIB-written test wire is re-

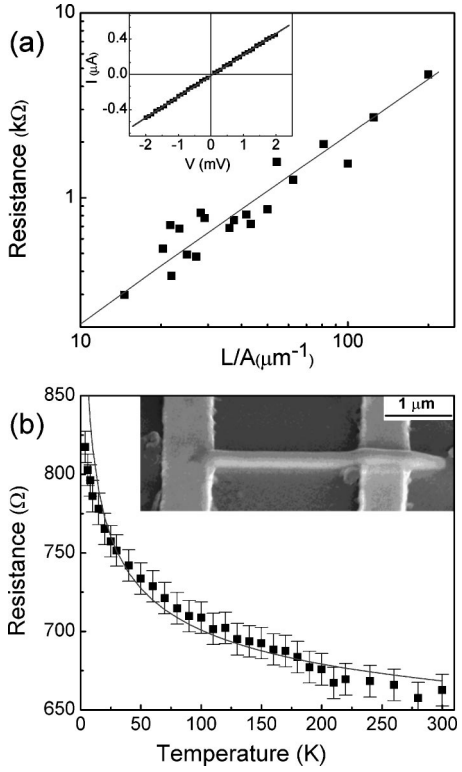

FIG. 3. (a) Measured resistance values of 20 single FIB wires bridging microelectrodes plotted vs the length/cross-sectional area ratio (L/A); from the slope of the fitting curve (solid line) the FIB-written wire resistivity can be extracted ($\rho_{\mathrm{FIB}}=2200\pm100\ \mu\Omega$ cm). Inset: room-temperature $I-V$ characteristic of a FIB test wire. The linear fit demonstrates ohmic behavior; (b) resistance of a 2-μm-long FIB-written test wire measured as a function of temperature. The solid line represents a fit to the 3D variable-range hopping model (VRH), where $R_{\mathrm{FIB}}(T)=R_0\exp[(T_0/T)^{1/4}]$. Inset: SEM image of a FIB test wire bridging parallel Au microelectrodes.

ported. As for the previous analysis, the value of a FIB-written wire resistivity (ρ_{FIB}) was extracted from the slope of the linear fit in Fig. 3(a). A value of the $\rho_{\mathrm{FIB}}=2200\pm100\ \mu\Omega$ cm, comparable to literature reports, was obtained.[9,11–13] This large resistivity value is expected because the FIB deposition method normally results in the formation of a disordered metallic compound containing Pt (30%), C (~70%) from the precursor gas (methylcyclopentadienyl-trimethyl platinum), contaminated with Ga from the ion beam, and O from the chamber (background pressure: 5.5×10^{-7} mbar).[9] From the fit intercept value it is found that the contact resistance between the FIB-deposited compound and the underlying microelectrodes is less than 80 Ω. The temperature dependence of the resistance of a FIB-written test wire, $R_{\mathrm{FIB}}^{\mathrm{meas}}(T)$, is plotted in Fig. 3(b), clearly showing a nonmetallic transport behavior ($\partial\rho/\partial T<0$) down to 4 K. This type of conduction behavior has been observed in a wide variety of disordered materials, in which the resistance curves were fitted to a variable range hopping (VRH) model.[14–19]

The R/T curve of Fig. 3(b) was indeed successfully fitted to a three-dimensional (3D) VRH model, described in Eq. (1) as follows:

$$R_{\mathrm{FIB}}(T)=R_\infty e^{\left(\frac{T_0}{T}\right)^{1/4}}, \tag{1}$$

in which R_∞ is the resistance for higher temperatures, and

$$T_0=\frac{18}{k_B\xi_L^3 N(E_{\mathrm{F}})}, \tag{2}$$

where k_B is the Boltzmann constant, ξ_L is the localization length, and $N(E_{\mathrm{F}})$ is the density of states at the Fermi energy.[15,20,21] From the fit, the values of $R_\infty=576\pm5\ \Omega$ and $T_0=0.15\pm0.02$ K were obtained. By assuming a rough estimate of $N(E_{\mathrm{F}})$ ($\approx10^{29}$ eV^{-1} m^{-3} for Pt), a localization length of $\xi_L\approx20$ nm was calculated in Eq. (2).[22] It should be pointed out that $N(E_{\mathrm{F}})$ is not precisely known because—as stated earlier—the deposited compound also contains C, Ga, and O in a variable concentration. These contamination elements should lower the value of $N(E_{\mathrm{F}})$, thus increasing ξ_L,. Similar values for T_0 and for ξ_L have been reported for ordered quasicrystals of I-AlPdRe ($T_0\sim1$ mK and $\xi_L\sim300$ nm).[19]

Within the framework of the Anderson theory of localization, the calculated value of ξ_L implies that the one-electron wave functions are no longer delocalized over the entire wire, but rather decay exponentially over a distance of the order of ξ_L.[23] This means that the disorder inside the FIB-deposited compound is large enough to "trap" the carriers into localized states, from which they may escape by thermally activated hopping conduction. Although Eq. (1) is only strictly valid for $\xi_{\mathrm{hop}}\gg\xi_L$, where ξ_{hop} is the VRH distance given by $\xi_{\mathrm{hop}}\cong0.4\xi_L(T_0/T)^{1/4}$), it has been shown, however, that the valid range of Eq. (1) can be extended for the case of $\xi_L\gg\xi_{\mathrm{hop}}$, where corrections to Mott's calculation gave the same exponential dependence of the conductivity, and only the pre-exponential factor R_∞ was affected.[17,19,24]

B. Evaluation of the intrinsic nanowire resistance

Figure 4(a) shows the measured temperature dependence of the resistance R_{meas} of a FIB-contacted 70-nm-diameter Pt NW device in the range 4–300 K. The device behavior is clearly metallic down to 20 K (filled circles). Below 20 K, however, the resistance increases. This low-temperature behavior might be attributable either to the contacts or to the NW itself. The measured NW room-temperature resistivity is 33 $\mu\Omega$ cm (well below the Mooij limit for disordered metals: 150 $\mu\Omega$ cm), suggesting that the increasing measured resistance below 20 K can be attributed to the nonmetallic nature of the FIB junction contacts.[25] The measured resistance may be described by the sum of $R_{\mathrm{meas}}(T)=R_{\mathrm{NW}}(T)+R_{\mathrm{track}}+R_{\mathrm{FIB}}(T)$. As previously discussed in Sec. IIIC, the room-temperature resistance of the FIB junction contacts (R_{FIB}) is estimated to be 275 Ω. The temperature dependence of R_{FIB} is accounted for by rescaling the characteristic of the measured FIB-written test wire, $R_{\mathrm{FIB}}^{\mathrm{meas}}(T)$, such that $R_{\mathrm{FIB}}^{\mathrm{meas}}(300\ \mathrm{K})=275\ \Omega$, and then subtracting this contribution (plus R_{track}) may then be subtracted from $R_{\mathrm{meas}}(T)$ in order to extract the NW resistance $R_{\mathrm{NW}}(T)$. The result of this analysis is depicted in Fig. 4(b) (empty circles).

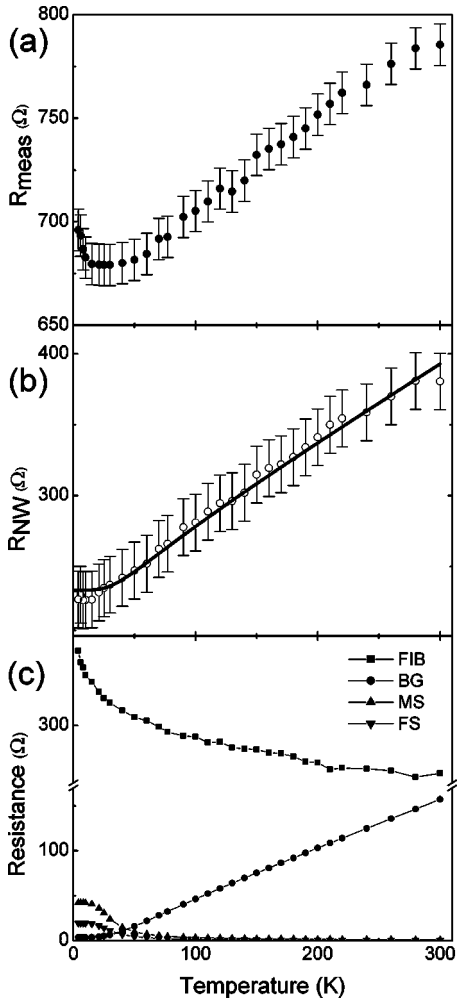

FIG. 4. (a) Resistance of a FIB contacted Pt NW, R_{meas}, measured as a function of temperature (filled circles); (b) the intrinsic NW resistance, R_{NW}, can be calculated at each temperature (open circles) by subtracting the contributions of the underlying microelectrodes and the FIB-written junction contacts. The solid line represents the fit to the combined BG-FS-MS model; (c) separation of the different contributions to $R_{meas}(T)$. Legend: (■) Estimated FIB resistance, (●) electron-phonon interaction (BG model), (▲) grain boundary scattering (MS model), and (▼) surface scattering (FS model).

C. Discussion

We first fit the intrinsic NW resistance data, R_{NW}, to the well-known Bloch-Gruneisen (BG) formula for classical metals,

$$R_{BG}(T) = R_0 + R_1 T\left(\frac{T}{\Theta_D}\right)^4 \int_0^{\Theta_D/T} \frac{x^5}{(e^x-1)(1-e^{-x})}dx, \tag{3}$$

in which R_0 is the residual resistance, R_1 is the temperature coefficient for the resistance, and Θ_D is the Debye temperature.[26] The Θ_D extracted from the fit, 118 K, is very close to the surface Debye temperature for Pt (surface value: 110 K; bulk value: 230 K), even though the wire diameter is 70 nm, i.e., a substantial scattering contribution from the bulk phonons is still expected.[27,28] This result, together with the enhanced room-temperature resistivity value (33 $\mu\Omega$ cm) suggests that additional physics is still required to explain the temperature dependence of the wire resistance. Although electron-phonon and impurity scattering—described by the BG model—is the dominant process in the system, scattering contributions from the NW surface and grain boundaries within the polycrystalline wire are also expected. The residual resistance ratio [RRR, where RRR $=R(300\text{ K})/R_0$] is found to be RRR=1.5, a value comparable with those reported for other metallic NWs.[3,4] This decreased RRR (relative to polycrystalline platinum) is a clear indication of the existence of the grain-boundary scattering within the electrodeposited Pt NWs.[29] Similar effects have also been found in epitaxial Co/Ni superlattices, in which the residual resistivity was observed to increase with decreasing overall film thickness in the range $d<50$ nm.[30]

Size effects can be taken into account by two theories: the Fuchs and Sondheimer theory (FS) for surface scattering, and the Mayadas and Shatzkes model (MS) for grain-boundary scattering.[31,32] An approximate formula for the FS model for wires with circular or quadratic cross section is given by

$$\frac{R_{FS}}{R_{BG}} = 1 + \frac{3}{4}(1-p_{FS})\frac{\lambda}{d}, \tag{4}$$

where p_{FS} is the probability of an electron to be scattered specularly at the surface, d is the diameter of the wire, and λ is the mean free path.[33] From the MS theory, the grain-boundary component to the resistivity is given by

$$\frac{R_{MS}}{R_{BG}} = \frac{1}{1-\frac{3}{2}\alpha+\alpha^2-\alpha^3\ln\left(1+\frac{1}{\alpha}\right)}, \tag{5}$$

where $\alpha=(\lambda/D_{gr})(R_{gr}/1-R_{gr})$, D_{gr} is the average dimension of the grains, and R_{gr} is the fraction of electrons not scattered by the potential barrier at a grain boundary.[33]

Following Steinhögl *et al.*, BG, FS, and MS models are combined by adding the resistances, neglecting deviations from the Matthiessen rule that may be expected in the presence of grain-boundary scattering.[33] The intrinsic NW resistance data, $R_{NW}(T)$ shown in Fig. 3(b), extracted from the measured device data [Fig. 3(a)] as described previously, is then fitted with the combined FS+MS+BG expression [solid line in Fig. 4(b)]. Within this framework, the different contributions to the measured resistance can be separated [Fig. 4(c)]. From this model, we find $\Theta_D=195$ K. The value is lower than the bulk value because the lattice at the wire surface vibrates more easily, due to the surface atoms having fewer nearest neighbors. As a consequence, the higher-energy phonons soften within the NW, and Θ_D is reduced. Similar effects have also previously been observed for thin Au films deposited on amorphous substrates and in Co/Ni superlattices.[30,34]

In the combined model, the temperature dependence of the resistance is contained in the mean free path, λ. The number of charge carriers is assumed constant; thus, the product $\lambda(T)\rho(T)$ should be a constant. In the curve fitting, this value was kept as a free parameter. From the fit, it is found that $[\lambda(T)\rho(T)]_{Pt}=8\times10^{-11}\ \Omega\ \text{cm}^2$, in good agreement with the value reported by Fischer *et al.* for 2 nm thick

Pt films (2×10^{-11} Ω cm^2).[35] In our NW, an enhanced value for the quantity $[\lambda(T)\rho(T)]_{Pt}$ is reasonable because the number of carriers is greater than in ultrathin films, due to the fact that a lower-defect density is expected. The fit result for the specular scattering coefficient is $p_{FS}=0.177$, very close to the values reported by Fischer *et al.* (0.13–0.15), and the grain-boundary reflection coefficient $R_{gr}=0.227$, is comparable with the values obtained for thin Au films (0.295), for Cu (0.24), and for Al (0.17).[32,34,35] The mean average grain diameter extracted from the fit is 21 nm, consistent with measured grain sizes (20–30 nm) in HRSEM images. This combined model allows the relative magnitude of the grain-boundary and the surface-scattering contributions to be estimated: grain-boundary scattering dominates over surface scattering at all temperatures by a factor of two.

V. CONCLUSIONS

These results demonstrate that FIB presents a rapid and flexible method for making stable, low-resistance ohmic contacts to single metal NWs for testing their electrical properties over a wide temperature range (4–300 K). The linear NW current–voltage characteristics were measured for current densities up to 65 kA/cm^2. The measured NW room-temperature resistivity (33 $\mu\Omega$ cm) indicates contributions due to surface- and grain-boundary scattering in the NWs. The fits of the temperature dependence of the extracted intrinsic NW resistance suggest that electron-phonon scattering is the dominant mechanism at all temperatures, but scattering contributions from the NW surface and grains cannot be neglected. FIB-written junction contacts may therefore be considered as an alternative to lithographically defined overlaid microelectrodes for electrically contacting metallic nanowire devices.

ACKNOWLEDGMENTS

The authors thank J. Greer and P. Delaney for helpful discussions, and L. Floyd and D. O'Connell for technical help during the acquisition of experimental data. This work was supported by the EU as part of the RTN project Micro-Nano (HPRN-CT-2000-00028), and by the Irish HEA PRTLI Nanoscale Science and Technology Initiative.

[1] S. Asai and Y. Wada, Proc. IEEE **85**, 505 (1997); The International Technology Roadmap for Semiconductors, http://public.itrs.net
[2] N. I. Kovtyukhova and T. E. Mallouk, Chem.-Eur. J. **8**, 4355 (2002).
[3] P. A. Smith, C. D. Nordquist, T. N. Jackson, T. S. Mayer, B. R. Martin, J. Mbindyo, and T. E. Mallouk, Appl. Phys. Lett. **77**, 1399 (2000).
[4] M. E. Toimil-Molares, E. M. Höhberger, Ch. Schaeflein, R. H. Blick, R. Neumann, and C. Trautmann, Appl. Phys. Lett. **82**, 2139 (2003).
[5] T. W. Ebbesen, H. J. Lezec, H. Hiura, J. W. Bennett, H. F. Ghaemi, and T. Thio, Nature (London) **382**, 54 (1996).
[6] S. B. Cronin, Y-M. Lin, O. Rabin, M. R. Black, J. Y. Ying, M. S. Dresselhaus, P. L. Gai, J-P. Minet, and J-P. Issi, Nanotechnology **13**, 653 (2002).
[7] B. Doudin, G. Redmond, S. E. Gilbert, and J.-Ph. Ansermet, Phys. Rev. Lett. **79**, 933 (1997); C. Schönenberger, B. M. I. Van der Zande, L. G. J. Fokkink, M. Henny, C. Schmid, M. Krüger, A. Bachtold, R, Huber, H. Birk, and U. Staufer, J. Phys. Chem. B **101**, 5497 (1997); C. R. Martin, Science **266**, 1961 (1993).
[8] C. Schönenberger, B. M. I. Van der Zande, L. G. J. Fokkink, M. Henny, C. Schmid, M.Krüger, A. Bachtold, R. Huber, H. Birk, and U. Staufer, J. Phys. Chem. B **101**, 5497 (1997).
[9] J.-F. Lin, J. P. Bird, L. Rotkina, and P. A. Bennett, Appl. Phys. Lett. **82**, 802 (2003).
[10] M. S. H. Go, *Focused ion beam fabrication of junctions in the charge density wave conductor $NbSe_3$*, M. Sc Thesis, TU Delft, 2000.
[11] K. A. Telari, B. R. Rogers, H. Fang, L. Shen, R. A. Weller, and D. N. J. Braski, J. Vac. Sci. Technol. B **20**, 590 (2002).
[12] T. Tao, J. Ro, J. Melngailis, Z. Xue, and H. D. Kaesz, J. Vac. Sci. Technol. B **9**, 2653 (1991).
[13] J. Melngailis and P. G. Blauner, Mater. Res. Soc. Symp. Proc. **147**, 127 (1989).
[14] R. C. Dynes and J. P. Garno, Phys. Rev. Lett. **46**, 137 (1981).
[15] V. Ravindranath M. S. Ramachandra Rao, G. Rangarajan, Yafeng Lu, J. Klein, R. Klingeler, S. Uhlenbruck, B. Büchner, and R. Gross, Phys. Rev. B **63**, 184434 (2001).
[16] M. Reghu, Y. Cao, D. Moses, and A. J. Heeger, Phys. Rev. B **47**, 1758 (1993).
[17] W. N. Shafarman, D. W. Koon, and T. G. Castner, Phys. Rev. B **40**, 1216 (1989).
[18] C. O. Yoon, M. Reghu, D. Moses, and A. J. Heeger, Phys. Rev. B **49**, 10851 (1994).
[19] J. Delahaye, J. P. Brison, and C. Berger, Phys. Rev. Lett. **81**, 4204 (1998).
[20] N. F. Mott and E. A. Davis, *Electronic Processes in Nanocrystalline Materials* (Oxford University Press, Oxford, 1979).
[21] N. F. Mott, *Metal-Insulator Transitions* (Taylor & Francis, London, 1990).
[22] F. Y. Fradin, D. D. Koelling, A. J. Freeman, and T. J. Watson-Yang, Phys. Rev. B **12**, 5570 (1975); O. K. Andersen, Phys. Rev. B **2**, 883 (1970).
[23] P. W. Anderson, Phys. Rev. **109**, 1492 (1958).
[24] N. F. Mott, J. Non-Cryst. Solids **1**, 1 (1968).
[25] J. H. Mooij, Phys. Status Solidi A **17**, 521 (1973).
[26] J. M. Ziman, *Electrons and Phonons* (Oxford University Press, Oxford, 1960).
[27] H. B. Lyon and G. A. Somorjai, J. Chem. Phys. **44**, 3707 (1966); B. Berembak, S. Zboray, B. Riedmuller, D. C. Papageorgopoulos, S. Stolte, and A. W. Klein, Phys. Chem. Chem. Phys. **4**, 68 (2002).
[28] N. W. Ashcroft and N. D. Mermin, *Solid State Physics* (Holt, Rinehart, and Winston, New York, 1976).
[29] *Handbook of Chemistry and Physics*, 76th ed., edited by David R. Lide (CRC, Boca Raton, FL, 1995-1996), Sec. 12, p. 47 , and references therein.
[30] S. Kim, H. Suhl, and I. K. Schuller, Phys. Rev. Lett. **78**, 322 (1997).
[31] K. Fuchs, Proc. Cambridge Philos. Soc. **34**, 100 (1938); E. H. Sondheimer, Adv. Phys. **1**, 1 (1952).
[32] A. F. Mayadas and M. Shatzkes, Phys. Rev. B **35**, 6453 (1987).
[33] W. Steinhögl, G. Schindler, G. Steinlesberger, and M. Engelhardt, Phys. Rev. B **66**, 075414 (2002).
[34] P. M. Th. M. van Attekum, P. H. Woerlee, G. C. Verkade, and A. A. M. Hoeben, Phys. Rev. B **29**, 645 (1984).
[35] G. Fischer, H. Hoffmann, and J. Vancea, Phys. Rev. B **22**, 6065 (1980).